Contents lists available at ScienceDirect

Chemical Engineering Research and Design

journal homepage: www.elsevier.com/locate/cherd

Power-saving airlift bioreactor with helical sieve plates: Developmental and performance studies

Xiang Li[b], *Yuqi Chen*[b], *Zhiyong Zheng*[a,c,*], *Minjie Gao*[b,**], *Zifan Wang*[b], *Kaining Zhang*[a], *He Liu*[a,c], *Xiaobei Zhan*[b]

[a] *Jiangsu Key Laboratory of Anaerobic Biotechnology, School of Environmental and Civil Engineering, Jiangnan University, Wuxi 214122, China*

[b] *Key Laboratory of Industrial Biotechnology of Ministry of Education, School of Biotechnology, Jiangnan University, Wuxi 214122, China*

[c] *Jiangsu Collaborative Innovation Center of Technology and Material of Water Treatment, Suzhou 215011, China*

ARTICLE INFO

Article history:
Received 18 September 2019
Received in revised form 28 February 2020
Accepted 9 March 2020
Available online 19 March 2020

Keywords:
Airlift reactor
Draft tube
Volumetric oxygen transfer coefficient
Gas holdup
Mixing time
Pichia pastoris

ABSTRACT

This study investigated the influence of the geometry of the draft tube on the mass transfer and energy efficiency in the airlift reactor with helical sieve plate (ALR-HSP). The power consumption efficiency was 46%–53% higher than the control condition by optimizing the draft tube. A set of empirical equations was used to describe the gas holdup and volumetric mass transfer coefficients corresponding to the geometry of draft tubes in the ALR-HSP for the water–air system. The comparative cultivation of *Pichia pastoris* was carried out using the ALR-HSP and the conventional airlift reactor (CALR). The biomass increased by 20%, the maximal specific growth rate during the logarithmic growth phase nearly doubled, and volumetric oxygen transfer coefficient increased by 21%–47% under the same culture conditions. Results preliminarily demonstrated the superior performance and practicability of the ALR-HSP in enhancing oxygen transfer efficiency and aerobic biological reaction efficiency.

Abbreviations: A_r, cross-section area of the riser (m^2); A_d, cross-sectional area of the downcomer (m^2); A_d/A_r, cross-sectional area ratio of the downcomer to riser; C*, saturated concentration of DO (%); C_0, initial concentration of DO (%); C_L, DO concentration read by the electrode (%); DO, dissolved oxygen (%); h_L, liquid level before aeration (m); h_g, liquid level during aeration (m); H/D, the ratio of the height of the draft tube to the diameter of the reactor; k_La, volumetric mass transfer coefficient (s^{-1}); k_La_S, volumetric mass transfer coefficient at the reference temperature S = 25 °C (s^{-1}); k_La_T, volumetric mass transfer coefficient at the tested *T* temperature (s^{-1}); k_La_L, overall volumetric mass transfer coefficient (s^{-1}); k_La_r, volumetric mass transfer coefficient in the riser section (s^{-1}); k_La_d, volumetric mass transfer coefficient in the downcomer section (s^{-1}); *P*, aeration power consumed by air compressor (kW); p_i, inlet pressure of the air compressor (bar); p_o, outlet pressure of air compressor (bar); Q_g, gas flow rate (m^3/s); *T*, temperature (°C); U_g, superficial gas velocity (m/s); V, liquid volume (m^3); τ_g, gas residence time (s); y_{O_2}, oxygen partial pressure (%, v/v); y_{CO_2}, CO_2 partial pressure (%, v/v); ε, overall gas holdup (%); τ, electrode response time (s); CER, CO_2 evolution rate (mmol/(L h)); OUR, oxygen uptake rates (mmol/(L h)); OTR, oxygen transfer rate (mmol/(L h)); ALR-HSP, airlift reactor with helical sieve plate; HSP, helical sieve plate; CALR, conventional airlift reactor.

* *Corresponding author at*: Jiangsu Key Laboratory of Anaerobic Biotechnology, School of Environmental and Civil Engineering, Jiangnan University, Wuxi 214122, China.

** *Corresponding author*.

E-mail addresses: zhiyong@jiangnan.edu.cn (Z. Zheng), jmgao@jiangnan.edu.cn (M. Gao).

https://doi.org/10.1016/j.cherd.2020.03.014

1. Introduction

The airlift reactor is developed on the basis of the bubble column (Merchuk and Gluz, 2002). This reactor uses gas sparging as the sole power source and relies on the draft tube to guide the circulation of multiphase flow and perform the gas–liquid mixing and mass transfer. The reactor is widely used in microbial fermentation (Michelin et al., 2013), wastewater treatment (Marques et al., 2007), and chemical reaction engineering (Pawar, 2016). Compared with the mechanical stirred tank reactor, the airlift reactor has the advantages of simple structure, power saving, and weakened shear force; however, it also has the disadvantages of less controllable parameters and relatively low mass transfer capacity (Michelin et al., 2013). Researchers have modified and optimized the internal configuration of the airlift reactor to improve the mass transfer efficiency and operation robustness (Räsänen et al., 2016; Sanjari et al., 2014). The modification of internal configuration in the airlift reactor can be divided into two categories (Table 1). One strategy is to control the initial bubble size to enhance the mass transfer rate, such as fine bubble diffusers (Sander et al., 2017), Venturi tube (Baylar et al., 2007), and fluidic oscillator (Hanotu et al., 2017). In general, the small initial bubbles are beneficial for improving mass transfer in the reactor (Al-Mashhadani et al., 2015). The other strategy is to interfere with the rising bubbles after they leave the distributor, such as setting the static mixer (Ghanem et al., 2014), the horizontal sieve plates (Luo et al., 2013), and the built-in vibration device (Elbing et al., 2016). The mass transfer rate has been improved by preventing the bubbles from coalescing and breaking the large bubbles to reduce the bubble size, change bubble shape, and prolong the bubble residence time (Chisti et al., 1995; Lukić et al., 2017; Luo et al., 2013). We can select various types of gas distributors and optimize the geometry and location of the draft tube for the internal configuration in airlift reactor. These adjustments can promote the mass transfer performance and save power consumption (Pawar, 2018). However, the development of the airlift reactor will be constrained by many factors, such as hygiene and sterilization requirement, fouling, crystal particle growth, and pore blockage, in different practical applications. For the pure microbial culture, complex internal configuration is prone to cause cleaning difficulties and contamination problems (Chisti and Moo-Young, 1994). The installation of the built-in static mixer can improve the mass transfer performance; however, the growth of the biofilm easily causes passage blockage, which impedes the successive mass transfer (Ghanem et al., 2014).

Recently, a novel airlift reactor with helical sieve plate (ALR-HSP) was developed by our research group (Zheng et al., 2018). This reactor can enhance the gas–liquid mass transfer rate and be used in aerobic fermentation processes. The previous work mainly focused on the influence of the structure of helical sieve plates (HSPs). The changes in mass transfer characteristics and power consumption with the variation in various geometric structures of the draft tube are still unclear. In the present work, the effect of the internal geometry on the oxygen transfer and aerobic microbial fermentation would be analyzed and verified by comparing the processes in the CALR and ALR-HSP. The relationship between experimental data and empirical equation would be constructed and preliminarily applied in *Pichia pastoris* culture.

2. Material and methods

2.1. Experimental setup

The water–air experimental setup, as shown in Fig. 1a, was modified on the basis of the previously reported 120 L internal circulation airlift reactor (Zheng et al., 2018). The reactor with a total volume of 230 L consisted of a stainless elliptic head connected to a cylinder made of transparent plastic by flanges. The draft tube was supported by three legs of 100 mm in height and placed in the center of the reactor. The gas sparger was a loop steel tube with 20 pores that were evenly distributed over a diameter of 300 mm. The pores were upwardly opened and had a diameter of 1.5 mm each. The gas entered from the

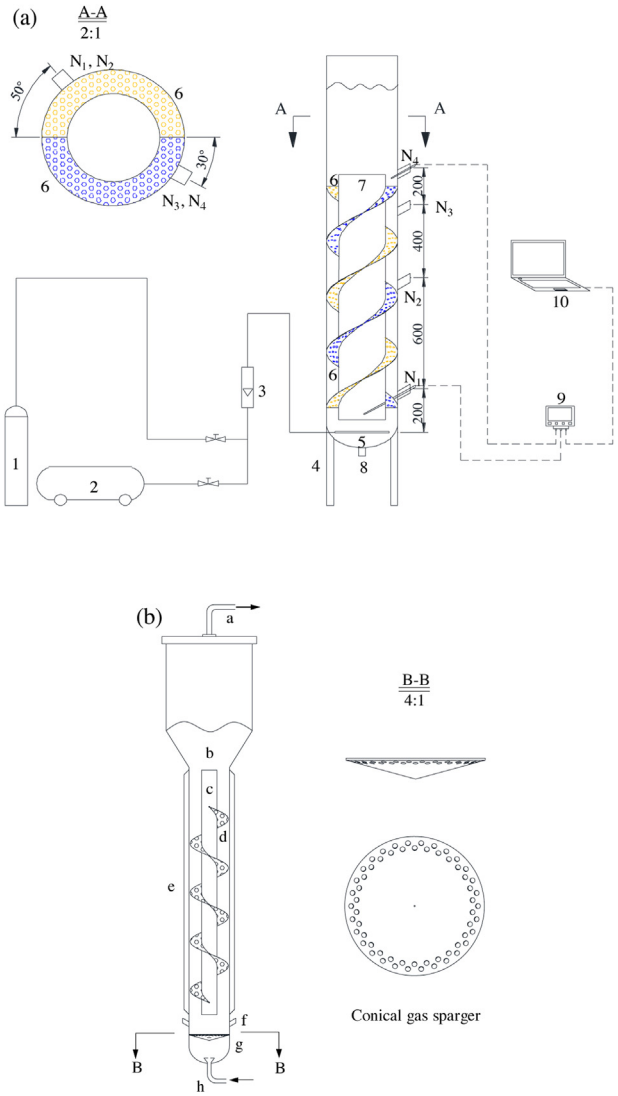

Fig. 1 – Schematics of (a) the 230 L ALR-HSP for water–air system, and (b) the 65 L ALR-HSP modified from Model SSTC for *P. pastoris* cultivation.
1-N_2, 2-air, 3-rotameter, 4-support legs, 5-gas sparger, 6-helical sieve plates, 7-draft tube, 8-outlet, 9-dissolved oxygen signal transmitter, 10-computer, N_1–N_4-electrode nozzles.
a-air outlet, b-gas–liquid separation zone, c-draft tube, d-helical sieve plate, e-cooling jacket, f-electrode nozzles, g-conical gas sparger, h-air inlet.

annulus (riser section) outside the draft tube, while the inside of the draft tube was the downcomer section. Table 2 shows the specifications and structural dimensions. Two sets of draft tubes were used in the experiment. The first set of draft tubes had the same height of 750 mm and various diameters of 160, 210, 240, and 260 mm. The second set of draft tubes had the same diameter of 240 mm and different heights of 750, 1050, and 1350 mm. The liquid level varied with the height of the draft tube and was kept 80 mm higher than the upper edge of the draft tube. As shown in Fig. 1a, the fixed site N_1 was used to measure k_La of the downcomer section. Meanwhile, sites N_2, N_3, and N_4 were used to measure k_La of the riser section with the draft tube height of 750, 1050, and 1350 mm, respectively. The free area ratio of the HSP was 63%. Table 2 shows the structural dimensions in detail. The experiment was carried out in tap water–air at room temperature. Water temperature

Table 1 – Internal configuration of airlift reactor and its characteristics.

Strategy	Internal configuration in airlift reactor	Characteristics	References
Control the initial bubble size	Loop tube with evenly distributed holes	Simple structure; Coarse initial bubbles; Often used in microbial aerobic fermenter.	Luo et al. (2011)
	Membrane disc/tube diffuser	Fine initial bubbles; Flexible membrane, not easy clogging; Prone to breakage after fatigue; Often used in aeration tank for wastewater.	Libra et al. (2005), Wei et al. (2014)
	Sintered ceramic/stainless steel plate	Fine initial bubbles; Easy clogging Could be autoclaved.	Jia et al. (2011)
	Venturi tubes	In the form of gas flow drives the liquid; Gas pressure loss is evident.	Baylar et al. (2007)
	Fluidic oscillator	Fine initial bubbles; Bubbles are prematurely detached from the distributor by oscillator.	Al-Mashhadani et al. (2015), Zimmerman et al. (2011)
Interfere with the rising bubbles	Static mixer	Large bubble is broken into small bubbles; Unsuitable for the aerobic fermentation with high hygienic requirements.	Chisti et al. (1990)
	Horizontal sieve plates	Slow the bubble coalescence and promote bubble breakup; Prone to bubble blockage beneath the plates; The area between the multi-layer plates cannot be cleaned	Luo et al. (2013)
	Helical flow promoters	Tubular gas distributors were helically fixed on the surface of the draft tube; Fine bubbles sprayed from the helical flow promoter improve the oxygen transfer performance.	Räsänen et al. (2016), Särkelä et al. (2019)
	Built-in vibration device	Bubble column reactor with vibration; Improve oxygen transmission performance with additional mechanical power input.	Elbing et al. (2016)
	Helical sieve plate	Prevents bubble coalescence and promotes bubble breakup; Hygienically clean-ups and is scalable.	Zheng et al. (2018)

Table 2 – Structure parameters of ALR-HSP for water–air system and aerobic fermentation.

Reactor parameters	Water–air system (mm)	Aerobic fermentation (mm)
Total reactor height of vessel	2130	1715
Reactor inner diameter	370	160
Inner diameter of gas–liquid separation zone	–	347
Draft tube height	750, 1050, 1350	1000
Ratio of the height of the draft tube to the diameter of the reactor.	2.03, 2.84, 3.65	6.25
Height of the HSPs	600, 900, 1200	800
Height of draft tube support leg	100	190
Draft tube outer diameter	160, 210, 240, 260	63
Cross-sectional area ratio of downcomer to riser	0.20, 0.43, 0.67, 0.90	0.16
Draft tube thickness	5	2
Distance from the liquid surface to the upper edge of the draft tube	80	80
Distance between the lower edges of HSP and the draft tube	60	50
Pitch of the HSP	600	200
Spacing between adjacent HSPs	300	200
Conical gas sparger diameter	–	160
Taper angle of conical gas sparger	–	150°

was measured before the experiment, and the experimental data were temperature calibrated as indicated in Section 2.2.2.

The ALR-HSP used for *P. pastoris* culture was modified from the 65 L airlift reactor (Model SSTC produced by Bioengineering AG, Switzerland). A set of self-designed draft tube, HSPs, and gas sparger was added to the airlift reactor, as shown in Fig. 1b. The free area ratio of the HSP was 61%. Central aeration in the draft tube was originally designed for the airlift reactor Model SSTC; thus, the riser section was also in the draft tube. A conical surface shaped gas distributor was installed among the legs of the draft tube to install an HSP and change the riser section to the annulus region in the reactor. Two rows of small holes of 5 mm were evenly distributed at the edges of the conical surface, as shown in Fig. 1b. Table 2 shows the structural dimensions of the experimental reactor in detail.

2.2. *Mass transfer characteristics*

2.2.1. *Gas holdup and residence time*

The gas holdup (ε) is defined as the proportion of the gas phase in the gas–liquid fluid. It was measured by the volume expansion method (Gavrilescu and Tudose, 1996). Liquid level was difficult to read accurately when the fluid was gassed. A high-speed camera was used to instantaneously record the

liquid level after the flow field stabilized. More than 50 photos were obtained to determine the liquid level, and the average reading was calculated. The overall gas holdup was calculated using Eq. (1). From Eq. (2), the gas residence time (τ_g) could be obtained.

$$\varepsilon = \frac{h_g - h_L}{h_g} \quad (1)$$

$$\tau_g = \frac{\varepsilon \cdot V}{(1-\varepsilon)Q_g} \quad (2)$$

where h_L is the liquid level before aeration (m), h_g is liquid level during aeration (m), V is liquid volume (m^3), and Q_g is gas flow rate (m^3/s).

2.2.2. Volumetric mass transfer coefficient

The volumetric mass transfer coefficient (k_La) was measured by dynamic method (Garcia-Ochoa and Gomez, 2009). Two dissolved oxygen (DO) electrodes (InPro 6800, Mettler Toledo) were installed in the riser and downcomer sections of the reactor, respectively, as shown in Fig. 1a and Section 2.1. The k_La values of the riser and downcomer sections were measured simultaneously. First, nitrogen gas was introduced at a high flow rate, and the oxygen in the liquid was removed until the DO reading was less than 5%. Then, the nitrogen gas was stopped, and the compressed air was switched at a preset flow rate. The connected control instrument automatically collected DO reading every 2 s until the DO reading reached 90% or higher. Considering the response time (τ) of the DO electrode (Garcia-Ochoa and Gomez, 2009) and the temperature (T) of the water–air system were measured, k_La was calculated and calibrated using Eqs. (3) and (4).

$$\frac{C^* - C_L}{C^* - C_0} = \frac{exp(-k_La \cdot t) - k_La \cdot \tau \cdot exp(-t/\tau)}{(1 - k_La \cdot \tau)} \quad (3)$$

$$k_La_S = \frac{k_La_T}{1.024^{T-S}} \quad (4)$$

where C^* is the saturated concentration of DO (%), C_L is the DO concentration read by the electrode (%), C_0 is the initial concentration of DO (%), t is the time (s), τ is the electrode response time (s), k_La_T is the volumetric mass transfer coefficient (s^{-1}) at the tested T temperature (°C), and k_La_S is the volumetric mass transfer coefficient (s^{-1}) at the reference temperature S = 25 °C.

The overall volumetric mass transfer coefficient in the reactor was calculated using Eq. (5).

$$k_La_L = k_La_r \times \left(\frac{A_r}{A_r + A_d}\right) + k_La_d \times \left(\frac{A_d}{A_r + A_d}\right) \quad (5)$$

where k_La_L is the overall volumetric mass transfer coefficient (s^{-1}), k_La_r is the volumetric mass transfer coefficient (s^{-1}) in the riser section, k_La_d is the volumetric mass transfer coefficient (s^{-1}) in the downcomer section, A_r is the cross-section area (m^2) of the riser, and A_d is the cross-section area (m^2) of the downcomer.

2.2.3. Mixing time

The mixing time (t_m) was measured by acid–base neutralization method. After the gas flow rate was stabilized, 40 mL of 1% (w/v) phenolphthalein solution and 50 mL of 1.0 mol/L NaOH solution were added to the reactor. When the solution became evenly magenta, 50 mL of 0.5 mol/L H_2SO_4 solution was added and the timing began. The color change of the solution was observed until the solution in the reactor became colorless. The counted duration time was the mixing time.

2.2.4. Aeration power

The power consumption of the airlift reactor comes from the air compressor. Thus, the aeration power could be calculated according to Eq. (6) described by Benz (2003).

$$P = \frac{5.97}{60} \times p_i \times Q_g \times \left[\left(\frac{p_o}{p_i}\right)^{0.283} - 1\right] \quad (6)$$

where P is the aeration power consumed by air compressor (kW), p_i is the inlet pressure of the air compressor (bar), p_o is the outlet pressure of air compressor (bar), and Q_g is the gas flow rate (m^3/s).

2.3. Microorganism and culture methods

2.3.1. Strain and media

P. pastoris KM71 was purchased from the Invitrogen Corporation. Yeast extract–peptone–dextrose (YPD) agar medium contained 10 g/L yeast extract, 20 g/L glucose, 20 g/L tryptone, and 20 g/L agar. YPD seed medium contained 10 g/L yeast extract, 20 g/L glucose, and 20 g/L tryptone. Fermentation medium contained 26 g/L glycerol, 1.0 g/L K_2SO_4, 1.0 g/L $MgSO_4$, 0.1 g/L $CaSO_4$, 20.0 g/L KOH, 5.0 g/L $(NH_4)_2SO_4$, 10 mL/L PTM1 trace salts, and 2.0% (v/v) H_3PO_4 under pH 6.0. The pH adjuster was 12% (v/v) aqueous ammonia. Antifoaming agent was diluted to 20% (v/v) from concentrated nonionic T-F composite-type antifoaming agent (Sangon Biotech, China). When plenty of foam was found on the liquid surface, the antifoaming agent was manually added. After each 0.5 mL addition, the antifoaming performance was observed and checked until the foam no longer grew.

2.3.2. Culture methods

The inoculum of *P. pastoris* was streaked on the YPD agar medium and cultured in a 30 °C incubator for 2 days. A single colony was inoculated in the 50 mL YPD in 500 mL shaker flask at 30 °C, 220 rpm for 16–24 h, and grew until OD_{600} reached 2.0. For the modified SSTC- type 65 L airlift reactor, a 5% (v/v) of inoculum was added into 28.5 L initial fermentation medium. The temperature was kept at 30 °C, the pH was maintained at 6.0 with 12% aqueous ammonia, and the aeration flow rate was 30 L/min.

2.4. Analytical methods

2.4.1. Cell concentration determination

The cell concentration was measured by the dry cell weight method. Cell samples (10 mL) were centrifuged and washed with pure water and then dried at 105 °C until constant weight was obtained. The tubes were weighed, and the dry weights of the samples were calculated. Cell concentration was also measured by optical density measurements at 600 nm (OD_{600}). One unit of OD_{600} corresponds to a dry cell weight of 0.307 g/L.

2.4.2. Glycerol concentration

The residual glycerol concentration was measured by HPLC method. One milliliter of culture was centrifuged at 11,000 rpm for 3 min, and the supernatant was filtered through a 0.33 μm syringe filter for HPLC analysis. The HPLC system (Agilent 1100, Agilent Technologies Inc., USA) was equipped with

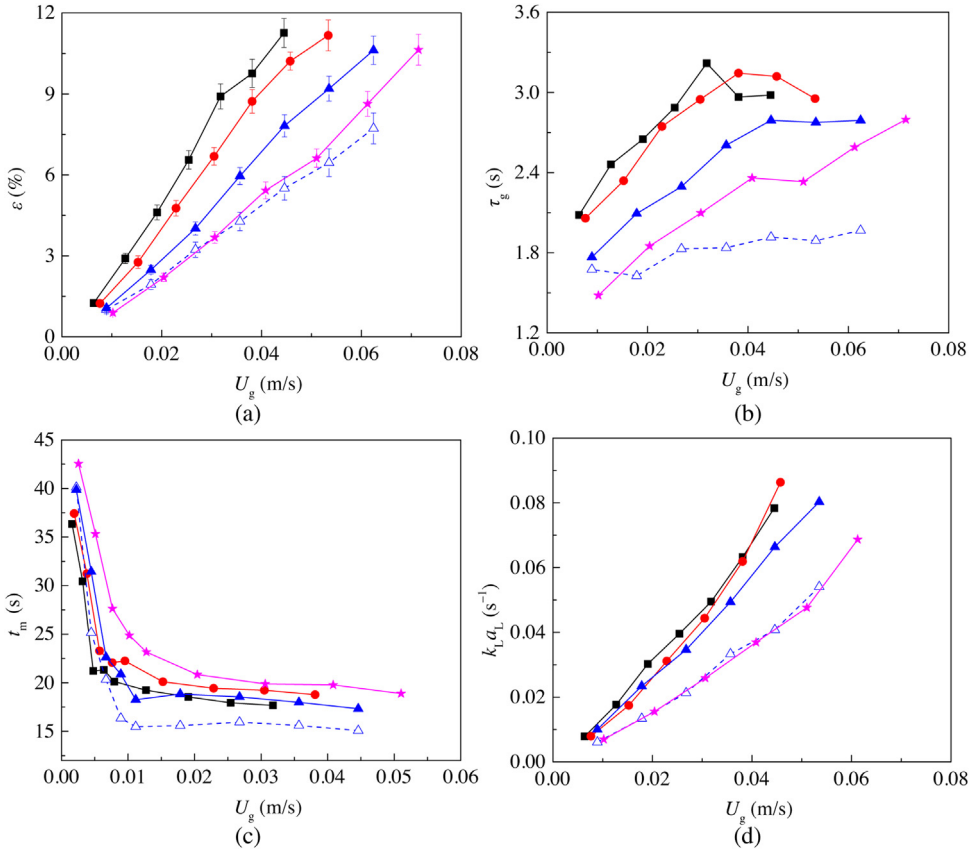

Fig. 2 – Effect of diameter of the draft tube on the oxygen transfer and mixing. (a) Gas holdup; (b) gas residence time; (c) mixing time; (d) overall volumetric oxygen transfer coefficient. (Solid line-ALR-HSP, dash line-CALR; ■-A_d/A_r = 0.20, ●-A_d/A_r = 0.43, ▲/△-A_d/A_r = 0.67, ★-A_d/A_r = 0.90).

a refraction index detector and an Aminex HPX-87H-Organic acid column (Φ7.8 mm × 300 mm). A constant flow rate of 0.6 mL/min mobile phase (5.0 mmol/L H_2SO_4) was applied to the HPLC column. The column was operated at 35 °C, and the sample injection volume was 20 μL.

2.4.3. NH_4-N content determination

NH_4-N content was measured by sodium salicylate–sodium hypochlorite colorimetric method (MEEC, 2009). The fermentation broth sample was centrifuged at 11,000 rpm for 3 min, and the supernatant was diluted 20 times with deionized water. Then, 0.2 mL of the diluted solution was taken, and 4 mL 5% (w/v) of sodium salicylate solution and 1.0 mL 0.14% (w/v) of sodium hypochlorite were added and mixed. The mixture was allowed to stand at room temperature for 12 min, and the absorbance was measured at 680 nm. Using anhydrous ammonium sulfate as a standard, the NH_4-N content was calculated according to the standard curve.

2.4.4. OUR, CER, and k_La during the aerobic fermentation

The O_2 and CO_2 partial pressured in the fermentation exhaust gas were measured by a gas analyzer (LKM2000A, Lokas Ltd., Korea). OUR, CER, and k_La were calculated using Eqs. (7) and (8). The calculation formula is shown as follows:

$$\mathrm{OUR} = \frac{Q_g}{22.4 \times 3.6 \times V} \times \left(0.21 - \frac{0.79 \times y_{O_2}}{1 - y_{O_2} - y_{CO_2}}\right) \times 1000 \quad (7)$$

$$\mathrm{CER} = \frac{Q_g}{22.4 \times 3.6 \times V} \times \frac{0.79 \times y_{CO_2}}{1 - y_{O_2} - y_{CO_2}} \times 1000 \quad (8)$$

$$k_La = \frac{0.145 \times \mathrm{OUR}}{C^* - C_L} \quad (9)$$

where OUR is the oxygen uptake rate (mmol/(L h)), CER is the CO_2 evolution rate (mmol/(L h)), Q_g is the gas flow rate (m^3/s), y_{O_2} is the oxygen partial pressure (%, v/v), y_{CO_2} is the carbon dioxide partial pressure (%, v/v), V is the liquid volume (m^3), k_La is the volumetric oxygen transfer coefficient (s^{-1}), C^* is the saturated concentration of DO (%), and C_L is the actual DO concentration (%).

3. Results and discussion

3.1. Effect of diameter of draft tube on oxygen transfer and mixing

The effects of various diameters of the draft tubes, that is, different cross-section area ratios of downcomer to riser sections (A_d/A_r), on mass transfer and mixing were investigated at the preset gas flow rates. The superficial gas velocity (U_g) is the ratio of the gas flow rate (Q_g) to the cross-sectional area of the riser section (A_r). Thus, different U_g values were generated at the same Q_g.

3.1.1. Gas holdup and residence time

The gas holdup of the reactor increased linearly with superficial gas velocity (U_g) at a fixed A_d/A_r. Meanwhile, the gas holdup increased with the decrease of the A_d/A_r at the same U_g (Fig. 2a). For a CALR, the gas holdup increased with the increase in Q_g (Bello et al., 1985). At the same U_g, the corresponding Q_g increased as A_d/A_r decreased, which resulted in

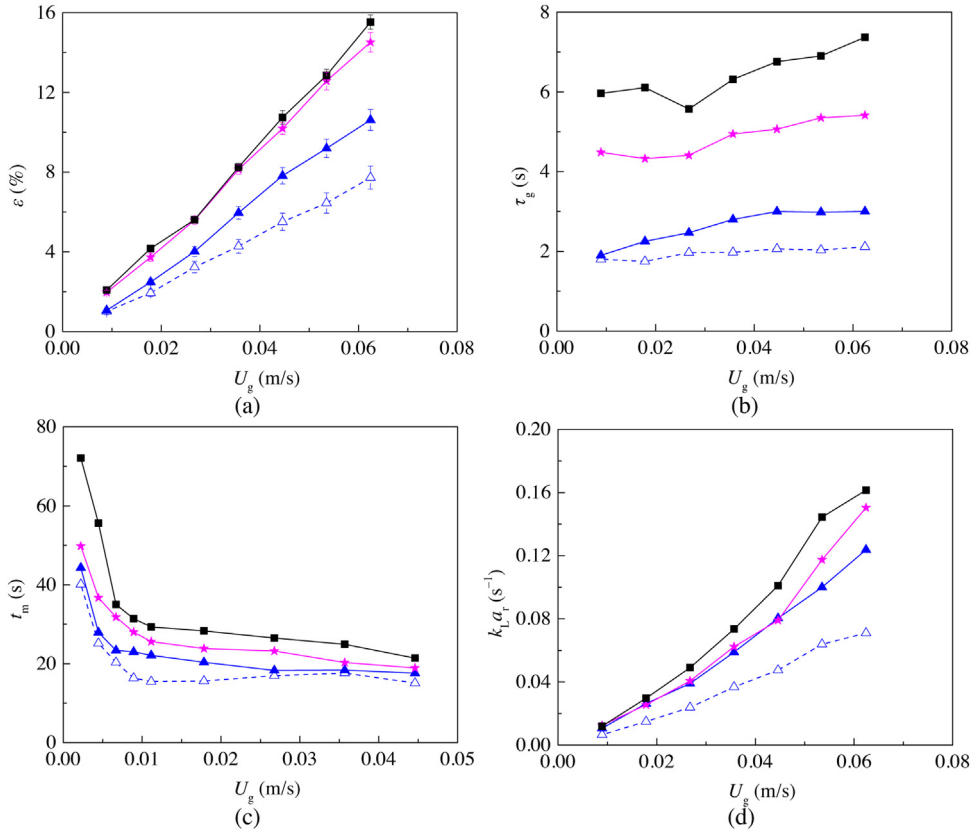

Fig. 3 – Effect of height of the draft tube on oxygen transfer and mixing. (a) gas holdup; (b) gas residence time; (c) mixing time; (d) volumetric oxygen transfer coefficient in the riser section. (Solid line-ALR-HSP, dash line-CALR; ▲/△ -*H/D* = 2.03, ★ -*H/D* = 2.84, ■-*H/D* = 3.65).

an increase in gas holdup. For the CALR with A_d/A_r = 0.67, the gas holdup in the reactor was lower than that of all the ALR-HSPs, in part owing to the many large bubbles were broken into small bubbles with the action of the HSP.

The gas residence time in the ALR-HSP was evidently longer than that of the CALR (Fig. 2b). First, some bubbles were guided by the HSPs to helically upward in the ALR-HSP, and their rising paths were lengthened. Second, some bubbles were impeded by the sieve plates and flew back. Finally, some bubbles were broken by the sieve plates and became smaller bubbles, which resulted in a decrease in the rising velocity. The above-mentioned mechanisms resulted in the long overall residence time of the bubbles and thus the increase in the gas holdup in the ALR-HSP.

3.1.2. *Mixing time*

The mixing time depends mainly on the dimension of the reactor and the flow pattern of the gas–liquid fluid, while the latter depends on the superficial velocity U_g and the hydraulic diameter. When U_g < 0.01 m/s (Fig. 2c), the flow pattern in the reactor could be determined as a homogeneous flow, at which condition the mixing time decreased sharply as U_g increased (Thobie et al., 2017). However, when U_g > 0.01 m/s, the flow pattern in the reactor was determined as a heterogeneous flow, and the mixing time nearly no longer changed with U_g (Thobie et al., 2017). Fig. 2c shows that the mixing time slightly shortened as A_d/A_r decreased. The reason might be that the liquid circulation velocity was increased as A_d/A_r decreased, that is, the cross-sectional area of the riser section increased; this condition reduced the mixing time (Wadaugsorn et al., 2016).

3.1.3. *Volumetric mass transfer coefficient*

Under different A_d/A_r conditions, the overall volumetric mass transfer coefficient (k_La_L) increased linearly with the increase in U_g (Fig. 2d). When A_d/A_r was in the range of 0.20–0.67, the difference in k_La_r values in the ALR-HSPs was insignificant at the same U_g. Under most conditions, the k_La_L values in the ALR-HSP were higher than those in the CALR. However, the k_La_L value in the ALR-HSP was relatively close to that in the CALR when A_d/A_r = 0.90. The reason was that the k_La value in the downcomer section was low, and the volume proportion was relative large, as a result, the k_La_L value decreased.

3.2. *Effect of height of draft tube on oxygen transfer and mixing*

The ratio of height to diameter (*H/D*) refers to the ratio of the height of the draft tube to the diameter of the reactor. This design parameter is important for the ALR. The change in *H/D* of the reactor causes a change in the reactor geometry and gas residence time, which in turn affects the mass transfer and mixing performance in the reactor.

3.2.1. *Gas holdup and residence time*

Fig. 3a shows the relationship between the gas holdup and U_g at various *H/D*. The gas holdup of the reactor increased linearly with the increase in U_g. The gas holdup in the ALR-HSP was significantly higher than that in CALR at the same *H/D*. Increasing the *H/D* of the reactor would increase the gas holdup of the reactor at the same U_g. When *H/D* was increased from 2.03 to 2.84, the gas holdup could be increased by 25%–41%. However, the increment in gas holdup would decrease as *H/D* increased further. The increase in *H/D* resulted

in a corresponding increase in the liquid level of the reactor. The displacement of the bubble from the gas distributor to the liquid level elongated with the impediment and breakup of the bubbles by the HSP, as a result, the gas residence time was prolonged (Fig. 3b). However, increasing the liquid level increased the bubble coalescence probability. Some small bubbles were merged into large bubbles, which accelerated the average rising velocity of the bubbles. This condition would reduce the gas residence time, which would reduce the gas holdup (Sanjari et al., 2014). The positive effect caused by the increase in *H/D* was greater than its negative effect, as a result, the gas holdup was significantly improved. However, the influence of the negative effect gradually became large when *H/D* was increased to a certain range. This condition reduced the increase in the gas holdup.

An equation of gas holdup including A_d/A_r (0.20–0.90), *H/D* (2.03–3.65), and U_g (0.009–0.062 m/s) in the ALR-HSP was established and fitted to the experimental data. The result was obtained as follows:

$$\varepsilon = 3.047U_g^{1.099}\left(\frac{1}{1+A_d/A_r}\right)^{1.412}\left(\frac{H}{D}\right)^{0.636}$$

$$R^2 = 0.986 \quad (10)$$

where U_g is the superficial gas velocity (m/s), *H/D* is the ratio of height of the draft tube to the diameter of the reactor, and A_d/A_r is the cross-sectional area ratio of the downcomer to riser.

The relationship between the fitted value and the experimental value was shown in Fig. S1a. The equation shows that the gas holdup was negatively correlated with A_d/A_r and positively correlated with *H/D*. The relationship between gas holdup and A_d/A_r was consistent with the results reported in Chisti and Moo-Young (2007). The relationship between the gas holdup and *H/D* was similar to that reported by Lu et al. (2000).

3.2.2. *Mixing time*

The mixing time prolonged as *H/D* increased (Fig. 3c). On the one hand, the increase in *H/D* led to a large liquid load and prolonged path of the liquid circulation. On the other hand, the bubble sparged from the gas distributor to the liquid level and needed to pass through sieve plates several times when *H/D* was increased, and the gas velocity was lowered, this condition prolonged the mixing time (Luo et al., 2013).

3.2.3. *Volumetric oxygen transfer coefficient*

As shown in Fig. 3d, k_La_r value increased with the increase in U_g at various *H/D*. The k_La_r value in the ALR-HSP increased slightly with the increase in *H/D* and was significantly higher than that in CALR at the same U_g. Mehrnia et al. (2004) reported similar results as above, but Sanjari et al. (2014) found that *H/D* negatively affected the k_La value of airlift reactor with a net draft tube. The slight positive effects observed in the present work might be due to two reasons. On the one hand, increasing *H/D* could prolong the gas residence time and facilitate complete contact between the gas and liquid phases. On the other hand, increasing *H/D* could increase the height of the draft tube and number of layers of HSP, which in turn could prolong the times of bubble breakup by the sieve plate.

The measured k_La values in the riser, the downcomer, and the overall reactor in ALR-HSP were functioned with A_d/A_r (0.20–0.90), *H/D* (2.03–3.65), and U_g (0.009–0.062 m/s), as fitted to the following equations:

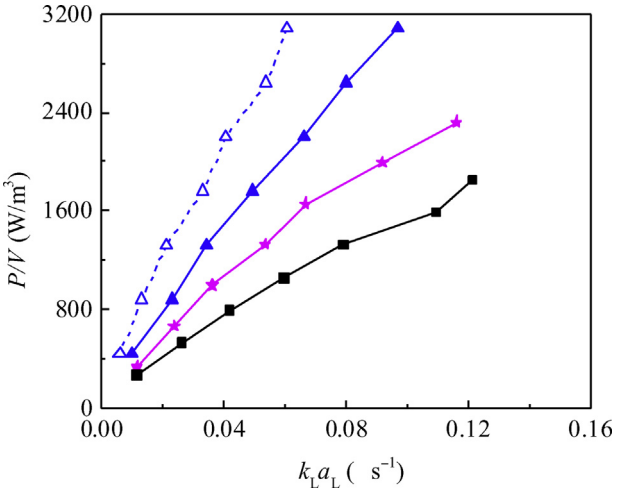

Fig. 4 – Relationship between the overall volume oxygen transfer coefficient and the power consumption per unit volume under various *H/D*. (solid line-ALR-HSP, dash line-CALR; ▲/△ -*H/D* = 2.03, ★ -*H/D* = 2.84, ■-*H/D* = 3.65).

$$k_La_r = 27.127U_g^{1.387}\left(\frac{1}{1+A_d/A_r}\right)^{1.069}\left(\frac{H/D}{H/D+1}\right)^{2.865}$$

$$R^2 = 0.962 \quad (11)$$

$$k_La_d = 3.312U_g^{1.111}\left(\frac{1}{1+A_d/A_r}\right)^{1.394}\left(\frac{H/D}{H/D+1}\right)^{0.359}$$

$$R^2 = 0.950 \quad (12)$$

$$k_La_L = 14.281U_g^{1.282}\left(\frac{1}{1+A_d/A_r}\right)^{1.264}\left(\frac{H/D}{H/D+1}\right)^{2.180}$$

$$R^2 = 0.970 \quad (13)$$

The relationship between the fitted value and the experimental value was shown in Fig. S1b, c, d. The sensitivity coefficients of k_La_r corresponding to U_g, *H/D*, and A_d/A_r were 1.300, 0.514, and −0.406, respectively, as calculated from Eq. (13). Eqs. (11) and (12) indicate that the k_La values in the riser and downcomer sections of the reactor were negatively correlated with A_d/A_r and positively correlated with *H/D*. Therefore, selecting a draft tube with large *H/D* and small diameter was conducive to the mass transfer process in the ALR-HSP.

3.2.4. *Power-saving performance of the ALR-HSP*

Fig. 4 shows the relationship between the power consumption per unit volume (P/V) and k_La_L in the reactors under various *H/D*. As indicated in Eq. (6), the air compressor power consumption was linearly proportional to Q_g under constant outlet pressure conditions. The k_La_L value of the reactor increased linearly with the increase in P/V. The k_La_L value of the reactors increased with the increase in *H/D*, and the k_La_L value of ALR-HSP was significantly larger than that of CALR at the same P/V. The power consumption of the airlift reactor was mainly from the gas supply unit. When the liquid level in the airlift reactor was increased, the inlet pressure of the

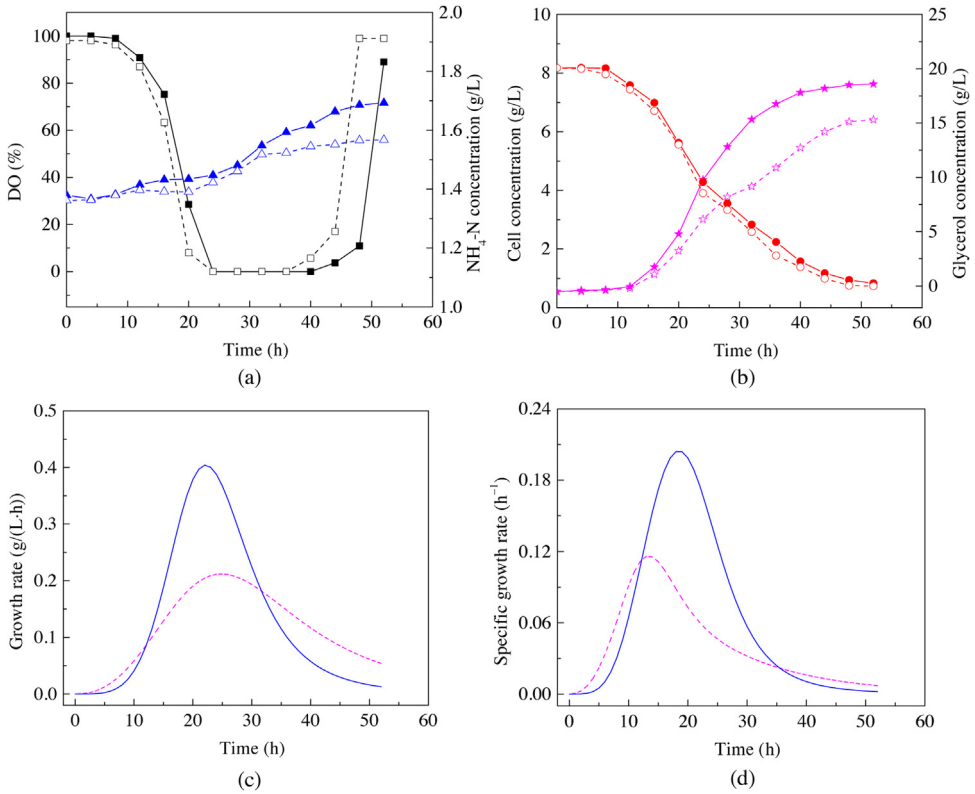

Fig. 5 – Process curves for the *Pichia pastoris* cultivation in the ALR-HSP and CALR. (a) DO and NH_4-N concentration; (b) cell and glycerol concentrations; (c) growth rate; (d) specific growth rate. (Solid line-ALR-HSP, dash line-CALR; ■/□-DO, ▲/△ -NH_4-N, ★/☆ -cell, ●/○ -glycerol).

gas due to hydrostatic pressure was increased linearly. However, the power consumption as a result was not improved proportionally with the inlet pressure of the gas for the condition of the same gas flow rate (Benz, 2019). Meanwhile, during the process of the gas ejecting from the sparger to the liquid surface for the actual aerobic fermentation, the oxygen takes up by the microorganisms accounted for only 1%–9% (Wei et al., 2016). Increasing *H/D* of the reactor resulted in the long gas residence time, which indicated that the microorganisms had high opportunities to use a great proportion of oxygen. Therefore, increasing *H/D* could evidently improve the power efficiency for the airlift reactors. Specifically, the k_La_L value in the ALR-HSP with *H/D* = 3.65 was improved by 46%–53% compared with that in the ALR-HSP with *H/D* = 2.03 for the same *P/V*. Compared with the efficiency for oxygen transfer ($k_La/(P/V)$) in the other airlift reactors that have been reported, the efficiency of oxygen transfer in the ALR-HSP with *H/D* = 3.65 was higher by 18%–80% than that in the external-loop airlift reactor (Lukić et al., 2017) and higher by 5%–17% than that in the airlift reactor occupied with helical flow promoters (Räsänen et al., 2016).

3.3. *Microbial aerobic fermentation in the ALR-HSP*

3.3.1. *Cell growth process*

DO is an important parameter in the aerobic fermentation process. In an airlift reactor, DO indicates the balance of oxygen supply and consumption and measures whether the oxygen limits the cell growth and metabolism. In the case of excessive Q_g, the microorganism culture system would generate a large amount of foam and cause the liquid loss. The addition of an appropriate amount of antifoaming agent could prevent excessive accumulation of foam. However, excessive addition also had an inhibition on the cell growth (Nielsen et al., 2017). On the basis of the preliminary pre-experiments for the *P. pastoris* cultivation, a constant flow rate of 30 L/min was selected (i.e., the same power consumption), and the total addition amount of the antifoaming agent was less than 0.5 mL/L.

Fig. 5a and b shows that the cell concentration and the oxygen demand were low when the cells grow in the lag phase of 0–12 h. The oxygen supply by the reactor was sufficient and the DO maintained constantly at a high level. The DO began to decline during 12–24 h, which indicated that the cell growth began to enter the logarithmic growth phase. During this period, the OUR increased rapidly (Fig. 6a), and the influence of the HSP on the DO gradually became evident. However, DO levels in the CALR and ALR-HSP were dropped to 0 at 24 h, at which time DO started to limit the cell growth, due to the limited oxygen supply capacity of the reactors. The glycerol concentration dropped below 2.5 g/L after 40 h and replaced the DO as a limiting substrate. The DO in the ALR-HSP first rose back and the CALR also followed, which indicated that the microorganism gradually entered a stationary phase. The biomass in ALR-HSP increased by approximately 20% compared with that in the CALR at the end of the fermentation. In the case of DO as the limiting substrate, the aerobic cultivation of *P. pastoris* with glycerol as a carbon source produced by-products, such as ethanol, arabitol, acetic acid, and pyruvic acid (Carnicer et al., 2009; Garcia-Ortega et al., 2013; Inan and Meagher, 2001). The accumulation of by-products would lead to a decrease in the yield coefficient of the biomass to the substrate, which might be the main reason for the low biomass concentration in the CALR. The pH value of the *P. pastoris* culture would be slightly decreased when glycerol was used as carbon source (Luo et al., 2018). Aqueous ammonia was added

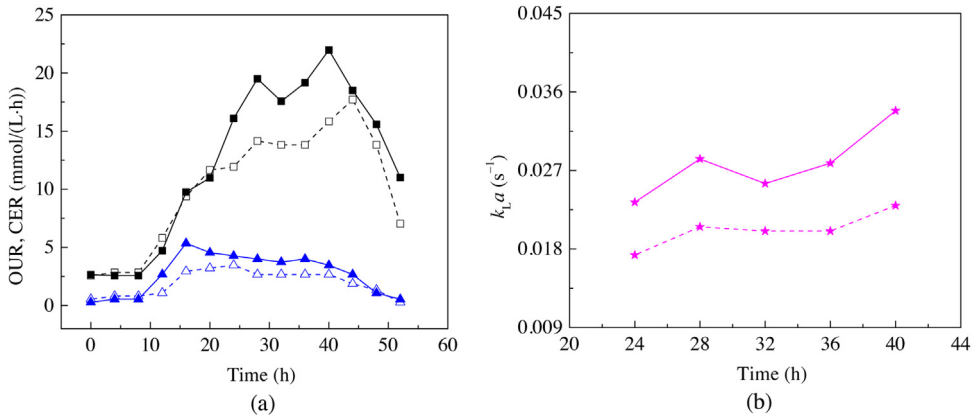

Fig. 6 – Comparison of OUR, CER, and k_La for *Pichia pastoris* cultivation in ALR-HSP and CALR. (a) OUR and CER; (b) k_La. (Solid line-ALR-HSP, dash line-CALR; ■/□-OUR, ▲/△ -CER, ★/☆ -k_La).

and maintained at pH 6.0; thus, NH_4-N concentration slowly increased during the fermentation process (Fig. 5a).

3.3.2. *Growth rate and specific growth rate*

The growth rate of the biomass is closely related to the rate of oxygen transfer rate (OTR) and the OUR, and the specific growth rate is related to the cell proliferation capacity and the concentration of limiting substrate (DO). The growth curve was fitted by Logistic equation and the time (*t*) was derived to obtain the growth rate and specific growth rate curves, as shown in Fig. 5c and d. Oxygen is an important nutrient substrate during microbial growth. A minimum limit of DO (DO_{min}) existed, and the cells were free to grow and were not limited by DO when DO > DO_{min}. When DO < DO_{min}, cell growth was limited by DO, at which time DO controlled specific growth rate and growth rate (Villadsen et al., 2011). Fig. 5c shows that the growth rate was low during the lag phase, and the growth rate increased rapidly after entering the logarithmic phase. The maximum oxygen supply capacity of the airlift reactors limited the cell growth rate during 24–40 h. The OTR in the ALR-HSP was higher than that in the CALR, as a result, the cell growth rate of the former was nearly doubled that of the latter (Fig. 5c). As shown in Fig. 5d, the difference in specific growth rate was maximized in the ALR-HSP and the CALR during the period of 12–20 h. The maximum specific growth rate of ALR-HSP was doubled compared with CALR. Furthermore, the evident difference in DO during 12–20 h (Fig. 5a) illustrated the superiority of the oxygen transfer performance of the ALR-HSP.

3.3.3. *OUR and CER*

Fig. 6a shows that OTR and CER began to increase in the two reactors after the 12 h lag period, which indicated that the cells growth started to accelerate. The OUR and CER tended to be constant during the 24–40 h, at which time low DO limited the growth rate. The OUR and CER began to decline after 40 h, and glycerol nearly depleted and limited cell growth, which resulted in a low OUR and CER. During the 24–40 h, the OUR and CER of ALR-HSP were significantly higher than CALR and increased by 27%–39% and 23–50%, respectively. The DO during the aerobic fermentation depends on OTR and OUR. The OUR depends on cell density, metabolic activity, and nutritional conditions. The OTR depends on the structure of the reactor, the operating conditions, and the physic-chemical properties of the fermentation broth. The gas flow rate Q_g was kept constant under the present experimental conditions. Thus, the OTR mainly depended on the reactor structure. OTR was equal to OUR when at the steady-state conditions. A high OUR in the microbial culture process corresponded to improved mass transfer performance in the bioreactor.

3.3.4. *Volumetric oxygen transfer coefficient*

The culture system was in stationary phase during the 24–40 h, at which time the OUR of the culture system was equal to OTR. The k_La value in the reactor could be calculated using Eq. (9). The k_La value in ALR-HSP was 21%–47% higher than that in the CALR (Fig. 6b). When the DO decreased to 0 (i.e., k_La = OUR/C_L^*), the change in k_La directly reflected the changes in OUR and OTR. Before the aerobic cultivation by using the ALR-HSP modified from 65 L Model SSTC, the k_La value was measured in water–air condition (Q_g = 30 L/min) to be 0.030 ± 0.005 s^{-1}. Meanwhile, the k_La value measured by the gas analyzer for the aerobic cultivation of *P. pastoris* was 0.029 ± 0.004 s^{-1}. The k_La values obtained by two different methods at the same gas flow rate were very close.

It was observed that more foam tended to accumulate on the liquid level of the ALR-HSP during the aerobic fermentation than that in the CLAR. The large bubbles were prone to be broken into some small bubbles with the action of HSP, thus the resulting small bubbles with stable thermodynamic state would be continuously accumulated on the liquid surface. This negative phenomenon was accompanied by the improvement of mass transfer, which requires our further research. The problem can be solved by coupling the anti-foaming assembly, such as centrifugal rotary plate foam breakers (Vetoshkin, 2003) and gas–liquid cyclone separator (Huang et al., 2018). In general, the mass transfer performance in the ALR-HSP was significantly improved compared with that in the CALR under the same power consumption. This finding has significant industrial value for improving the power efficiency in the airlift reactors.

4. Conclusions

The effects of the geometry of the draft tube (A_d/A_r, *H/D*) on the mass transfer and energy efficiency in ALR-HSP were investigated and the empirical correlations for the estimation of gas holdup and volumetric mass transfer coefficient were proposed. Reducing the diameter of the draft tube could increase the gas holdup, increase the gas residence time, and then improve the oxygen transfer efficiency. Increasing the height of the draft tube with a fixed spacing between adja-

cent HSPs could increase the number of layers of the HSPs. Thus the times that the bubbles passing through the HSP was increased and the size of the bubbles was reduced. With the constant gas flow rate and the increased liquid volume, the reactor maintained a high oxygen mass transfer efficiency which significantly improved the energy efficiency in ALR-HSP. *P. pastoris* aerobic fermentation was carried out for the first time in the novel ALR-HSP. The fermentation performance of ALR-HSP was significantly better than that of CALR under the same cultivation conditions. This further illustrates that ALR-HSP has high efficiency of mass transfer and power-saving performance. Compared with the airlift reactor with the horizontal sieve plates, ALR-HSP has the advantages of not being easily clogged by mycelial pellets and accessible to be cleaned and maintained. The novel ALR-HSP might have promising applications in algae microbial cultivation, syngas microbial fermentation, and Fischer–Tropsch synthesis.

Conflicts of interest

None.

Acknowledgments

Financial Supports from the National Natural Science Foundation of China (31271888), the Fundamental Research Funds for the Central Universities (JUSRP51632A), the National Key Research and Development Program of China (2017YFD0400302) are gratefully acknowledged.

Appendix A. Supplementary data

Supplementary material related to this article can be found, in the online version, at doi:https://doi.org/10.1016/j.cherd.2020.03.014.

References

Al-Mashhadani, M.K.H., Wilkinson, S.J., Zimmerman, W.B., 2015. Airlift bioreactor for biological applications with microbubble mediated transport processes. Chem. Eng. Sci. 137, 243–253.

Baylar, A., Ozkan, F., Unsal, M., 2007. On the use of venturi tubes in aeration. Clean Soil Air Water 35 (2), 183–185.

Bello, R.A., Robinson, C.W., Moo-Young, M., 1985. Gas holdup and overall volumetric oxygen transfer coefficient in airlift contactors. Biotechnol. Bioeng. 27 (3), 369–381.

Benz, G.T., 2003. Optimize power consumption in aerobic fermenters. Chem. Eng. Prog. 99 (5), 32–35.

Benz, G.T., 2019. Optimize aspect ratio in industrial fermenters. Chem. Eng. Prog. 115 (4), 26–31.

Carnicer, M., Baumann, K., Töplitz, I., Sánchez-Ferrando, F., Mattanovich, D., Ferrer, P., Albiol, J., 2009. Macromolecular and elemental composition analysis and extracellular metabolite balances of *Pichia pastoris* growing at different oxygen levels. Microb. Cell Fact. 8, 65–78.

Chisti, Y., Moo-Young, M., 1994. Clean-in-place systems for industrial bioreactors: design, validation and operation. J. Ind. Microbiol. 13 (4), 201–207.

Chisti, M.Y., Moo-Young, M., 2007. Airlift reactors: characteristics, applications and design considerations. Chem. Eng. Commun. 60 (1–6), 195–242.

Chisti, Y., Kasper, M., Moo-Young, M., 1990. Mass transfer in external-loop airlift bioreactors using static mixers. Can. J. Chem. Eng. 68 (1), 45–50.

Chisti, Y., Wenge, F., Moo-Young, M., 1995. Relationship between riser and downcomer gas hold-up in internal-loop airlift reactors without gas–liquid separators. Chem. Eng. J. 57 (1), b7–b13.

Elbing, B.R., Still, A.L., Ghajar, A.J., 2016. Review of bubble column reactors with vibration. Ind. Eng. Chem. Res. 55 (2), 385–403.

Garcia-Ochoa, F., Gomez, E., 2009. Bioreactor scale-up and oxygen transfer rate in microbial processes: an overview. Biotechnol. Adv. 27 (2), 153–176.

Garcia-Ortega, X., Ferrer, P., Montesinos, J.L., Valero, F., 2013. Fed-batch operational strategies for recombinant Fab production with *Pichia pastoris* using the constitutive *GAP* promoter. Biochem. Eng. J. 79, 172–181.

Gavrilescu, M., Tudose, R.Z., 1996. Effects of downcomer-to-riser cross sectional area ratio on operation behaviour of external-loop airlift bioreactors. Bioprocess. Eng. 15 (2), 77–85.

Ghanem, A., Lemenand, T., Della Valle, D., Peerhossaini, H., 2014. Static mixers: mechanisms, applications, and characterization methods—a review. Chem. Eng. Res. Des. 92 (2), 205–228.

Hanotu, J.O., Bandulasena, H., Zimmerman, W.B., 2017. Aerator design for microbubble generation. Chem. Eng. Res. Des. 123, 367–376.

Huang, L., Deng, S., Chen, Z., Guan, J., Chen, M., 2018. Numerical analysis of a novel gas–liquid pre-separation cyclone. Sep. Purif. Technol. 194, 470–479.

Inan, M., Meagher, M.M., 2001. The effect of ethanol and acetate on protein expression in *Pichia pastoris*. J. Biosci. Bioeng. 92 (4), 337–341.

Jia, Z., Kulick III, F.M., Koch, K., 2011. Impact of structured sheet media on the oxygen transfer efficiency of fine and coarse bubble diffusers. Proc. Water Environ. Fed. 11, 5191–5209.

Libra, J.A., Sahlmann, C., Schuchardt, A., Handschag, J., Wiesmann, U., Gnirss, R., 2005. Evaluation of ceramic and membrane diffusers under operating conditions with the dynamic off gas method. Water Environ. Res. 77 (5), 447–454.

Lu, X., Ding, J., Wang, Y., Shi, J., 2000. Comparison of the hydrodynamics and mass transfer characteristics of a modified square airlift reactor with common airlift reactors. Chem. Eng. Sci. 55 (12), 2257–2263.

Lukić, N.L., Šijački, I.M., Kojić, P.S., Popović, S.S., Tekić, M.N., Petrović, D.L., 2017. Enhanced mass transfer in a novel external-loop airlift reactor with self-agitated impellers. Biochem. Eng. J. 118, 53–63.

Luo, L., Liu, F., Xu, Y., Yuan, J., 2011. Hydrodynamics and mass transfer characteristics in an internal loop airlift reactor with different spargers. Chem. Eng. J. 175, 494–504.

Luo, L., Yuan, J., Xie, P., Sun, J., Guo, W., 2013. Hydrodynamics and mass transfer characteristics in an internal loop airlift reactor with sieve plates. Chem. Eng. Res. Des. 91 (12), 2377–2388.

Luo, Z., Miao, J., Luo, W., Li, G., Du, Y., Yu, X., 2018. Crude glycerol from biodiesel as a carbon source for production of a recombinant highly thermostable β-mannanase by *Pichia pastoris*. Biotechnol. Lett. 40 (1), 135–141.

Marques, P., Pinheiro, H.M., Rosa, M.F., 2007. Cd(II) removal from aqueous solution by immobilised waste brewery yeast in fixed-bed and airlift reactors. Desalination 214 (1–3), 343–351.

Mehrnia, M.R., Towfighi, J., Bonakdarpour, B., Akbarnegad, M.M., 2004. Influence of top-section design and draft-tube height on the performance of airlift bioreactors containing water–in–oil microemulsion. J. Chem. Technol. Biotechnol. 79 (3), 260–267.

Merchuk, J.C., Gluz, M., 2002. Bioreactors, air-lift reactors. In: Flickinger, M.C., Drew, S.W. (Eds.), Encyclopedia of Bioprocess Technology. John Wiley and Sons, Inc., New Jersey, pp. 281–304.

Michelin, M., Oliveira Mota, A.M., Polizeli, M.L.T.M., Silva, D.P., Vicente, A.A., Teixeira, J.A., 2013. Influence of volumetric oxygen transfer coefficient (k_La) on xylanases batch production by *Aspergillus niger* van Tieghem in stirred tank and internal-loop airlift bioreactors. Biochem. Eng. J. 80, 19–26.

Ministry of Ecology and Environment of the People's Republic of China, 2009. Water quality – determination of ammonia nitrogen – salicylic acid spectrophotometry. National Environmental Protection Standard of the People's Republic of China, HJ 536–2009.

Nielsen, J.C., Senne de Oliveira Lino, F., Rasmussen, T.G., Thykaer, J., Workman, C.T., Basso, T.O., 2017. Industrial antifoam agents impair ethanol fermentation and induce stress responses in yeast cells. Appl. Microbiol. Biotechnol. 101 (22), 8237–8248.

Pawar, S.B., 2016. Process engineering aspects of vertical column photobioreactors for mass production of microalgae. ChemBioEng Rev. 3 (3), 101–115.

Pawar, S.B., 2018. Computational fluid dynamics (CFD) analysis of airlift bioreactor: effect of draft tube configurations on hydrodynamics, cell suspension, and shear rate. Bioprocess Biosyst. Eng. 41 (1), 31–45.

Räsänen, M., Eerikäinen, T., Ojamo, H., 2016. Characterization and hydrodynamics of a novel helix airlift reactor. Chem. Eng. Process. 108, 44–57.

Sander, S., Behnisch, J., Wagner, M., 2017. Energy, cost and design aspects of coarse- and fine-bubble aeration systems in the MBBR IFAS process. Water Sci. Technol. 75 (4), 890–897.

Sanjari, S., Vahabzadeh, F., Naderifar, A., Pesaran, M., 2014. Hydrodynamics and mass transfer coefficients of airlift reactors with net draft tubes of different sizes: production of cyclodextrin glucano transferase using *Bacillus* sp. DSM 2523. Starch Stärke 66 (11–12), 935–946.

Särkelä, R., Eerikäinen, T., Pitkänen, J.-P., Bankar, S., 2019. Mixing efficiency studies in an airlift bioreactor with helical flow promoters for improved reactor performance. Chem. Eng. Process. 137, 80–86.

Thobie, C., Gadoin, E., Blel, W., Pruvost, J., Gentric, C., 2017. Global characterization of hydrodynamics and gas–liquid mass transfer in a thin-gap bubble column intended for microalgae cultivation. Chem. Eng. Process. 122, 76–89.

Vetoshkin, A.G., 2003. Modeling of centrifugal rotary plate foam breakers. Theor. Found Chem. Eng. 37 (4), 372–377.

Villadsen, J., Nielsen, J., Lidén, G., 2011. Bioreaction Engineering Principles, third ed. Springer, New York.

Wadaugsorn, K., Limtrakul, S., Vatanatham, T., Ramachandran, P.A., 2016. Hydrodynamic behaviors and mixing characteristics in an internal loop airlift reactor based on CFD simulation. Chem. Eng. Res. Des. 113, 125–139.

Wei, C., Wu, B., Li, G., Chen, K., Jiang, M., Ouyang, P., 2014. Comparison of the hydrodynamics and mass transfer characteristics in internal-loop airlift bioreactors utilizing either a novel membrane-tube sparger or perforated plate sparger. Bioprocess Biosyst. Eng. 37 (11), 2289–2304.

Wei, Y., Yin, X., Qi, L., 2016. Effects of carrier-attached biofilm on oxygen transfer efficiency in a moving bed biofilm reactor. Front. Environ. Sci. Eng. 10 (3), 569–577.

Zheng, Z., Chen, Y., Zhan, X., Gao, M., Wang, Z., 2018. Mass transfer intensification in a novel airlift reactor assembly with helical sieve plates. Chem. Eng. J. 342, 61–70.

Zimmerman, W.B., Zandi, M., Hemaka Bandulasena, H.C., Tesař, V., James Gilmour, D., Ying, K., 2011. Design of an airlift loop bioreactor and pilot scales studies with fluidic oscillator induced microbubbles for growth of a microalgae *Dunaliella salina*. Appl. Energy 88 (10), 3357–3369.